MNRAS **000**, 000–000 (0000) Preprint 28 January 2016 Compiled using MNRAS LATEX style file v3.0

A reappraisal of parameters for the putative planet PTFO 8-8695b and its potentially precessing parent star.

Ian D. Howarth*
Dept. of Physics and Astronomy, University College London, Gower Street, London WC1E 6BT, UK

Accepted 2016 January 27. Received 2016 January 23; in original form 2015 November 16

arXiv:1601.07540v1 [astro-ph.SR] 27 Jan 2016

ABSTRACT
Published photometry of fading events in the PTFO 8-8695 system is modelled using improved treatments of stellar geometry, surface intensities, and, particularly, gravity darkening, with a view to testing the planetary-transit hypothesis. Variability in the morphology of fading events can be reproduced by adopting convective-envelope gravity darkening, but near-critical stellar rotation is required. This leads to inconsistencies with spectroscopic observations; the model also predicts substantial photometric variability associated with stellar precession, contrary to observations. Furthermore, the empirical ratio of orbital to rotational angular momenta is at odds with physically plausible values. An exoplanet transiting a precessing, gravity-darkened star may not be the correct explanation of periodic fading events in this system.

Key words: stars: individual: PTFO 8-8695 – stars: planetary systems

1 INTRODUCTION

Although the number of confirmed exoplanets is now in the thousands, the discovery by van Eyken et al. (2012) of a possible hot Jupiter transiting the M-dwarf T-Tauri star PTFO 8-8695 is of particular interest. Not only is the system exceptionally young (∼3 Myr; Briceño et al. 2005), which is of significance in the context of timescales for planetary formation and orbital evolution, but also it exhibits variability and asymmetry in the transit light-curves observed in the two seasons of the Palomar Transient Factory Orion project (PTFO; van Eyken et al. 2011). While part of the variability may arise through intrinsic stellar effects (such as starspots), Barnes et al. (2013) offered an insightful and credible interpretation that requires precession of the orbital and rotational angular-momentum vectors on short timescales ($\sim 10^2$ d, to account for the variable transit depth) coupled with a significantly gravity-darkened primary (to generate the light-curve asymmetry).

Barnes et al. (2013) constructed a detailed numerical realisation of this model, including periodic precession, which reproduced the variable light-curve extremely well. Because of their interest in physically modelling the precession, they constrained their model fits by adopting specific values for the stellar mass; and in order to reduce the number of free parameters they assumed (with some observational justification) synchronous rotation. Kamiaka et al. (2015) relaxed this assumption, and showed that, while the system geometry at the two observed epochs is reasonably well determined, multiple plausible solutions of the intervening precessional motion exist (as had been anticipated by Barnes et al.). Both the Barnes et al. and the Kamiaka et al. models predict that, as observed, transits should not occur at some epochs, as a consequence of orbital precession.

Ciardi et al. (2015) have recently published follow-up observations which demonstrate further transit-like features in the light-curve with the correct orbital phasing, albeit at epochs not consistent with the specific precession model advanced by Barnes et al. (2013); but while this paper was being prepared, Yu et al. (2015) reported additional observations which challenge the Barnes et al. framework. Thus PTFO 8-8695b remains, at best, only a *candidate* planet. The purpose of the present note is to examine this issue through more-detailed modelling of the stellar emission, to test, in particular, the gravity-darkening hypothesis.

2 MODEL

2.1 Motivation

Both Barnes et al. (2013) and Kamiaka et al. (2015) adopted classical von Zeipel (1924) gravity darkening, in which the emergent flux is locally proportional to gravity; that is,

$$T_{\mathrm{eff}(\ell)} \propto g^{\beta}$$

with $\beta = 0.25$ (where $T_{\mathrm{eff}(\ell)}$ is to be understood as the *local* effective temperature).

However, von Zeipel's derivation was based on consideration of a barotropic envelope in which energy transport is diffusive – i.e., radiative. Lucy (1967) argued that for stars

* E-mail: i.howarth@ucl.ac.uk

© 0000 The Authors

with convective envelopes the gravity-darkening exponent β is expected to be considerably smaller; this argument certainly applies in the case of PTFO 8-8695 (spectral type ∼M3; Briceño et al. 2005).

Recent work suggests that von Zeipel's 'law' may overestimate gravity darkening even in radiative envelopes (Espinosa Lara & Rieutord 2011); and, while it may be argued that, in respect of convective envelopes, "nothing is clear" (Rieutord 2015), it is surely the case that the gravity-darkening exponent will be less than in radiative envelopes. The limited empirical evidence is broadly consistent with Lucy's estimate of $\beta \simeq 0.08$ (e.g., Rafert & Twigg 1980; Pantazis & Niarchos 1998; Djurašević et al. 2003, 2006), and it is this value that will be adopted here.

The best-fit parameters derived by Barnes et al. (2013; their Table 2)[1] imply a ratio of rotational angular velocity to the critical, or break-up, value of $\omega/\omega_c \simeq 0.70 \pm 0.04$, and thence an equatorial:polar temperature ratio of $\sim 0.90 \pm 0.02$. To achieve the same temperature contrast with $\beta = 0.08$ (and hence to achieve roughly the same degree of light-curve asymmetries) requires significantly more rapid rotation: $\omega/\omega_c \simeq 0.95 \pm 0.02$. Of course, any change in ω/ω_c leads to changes in the shape of the star (and has implications for the rotation period and the projected equatorial rotation velocity, $v_e \sin i_s$), so it is not necessarily obvious that a consistent solution to the light-curves can be achieved with a more plausible gravity-darkening exponent.

2.2 Implementation

To examine this issue, a modified version of the code for spectrum synthesis of rapidly rotating stars described by Howarth & Smith (2001) has been used. The code, ExoBush,[2] simply divides the rotationally distorted stellar surface into a large number of facets; evaluates the local temperature and gravity at each point; and sums the intensities $I(\lambda, \mu, T, g)$[3] to produce a predicted flux, taking into account occultation by an opaque, nonluminous transiting body of assumed circular cross-section (e.g., an exoplanet).

2.2.1 Spin-orbit geometry

The spin-orbit geometry is conveniently considered in a right-handed co-ordinate system defined by the angular-momentum vectors, as illustrated in Fig. 1. The convention adopted here is that the planetary-orbit and stellar-rotation angular-momentum vectors **o**, **s** lie in the xy plane, with their vector sum **L** defining the y axis. Stellar rotation is assumed to be prograde (a choice that is necessarily arbitrary, leading to ambiguities in several model parameters; cf. the caption to Fig. 3), and the inclination of the rotation axis to the line of sight is required to be in the range $0 \leq i_s \leq \pi/2$.

[1] 'The' radius tabulated therein is the equatorial value (Barnes, personal communication).
[2] The etymology may be elucidated by an internet search for 'a thousand points of light', which is, conceptually, how the tiling of the stellar surface is performed.
[3] Here $\mu = \cos\theta$, where θ is the angle between the surface normal and the line of sight.

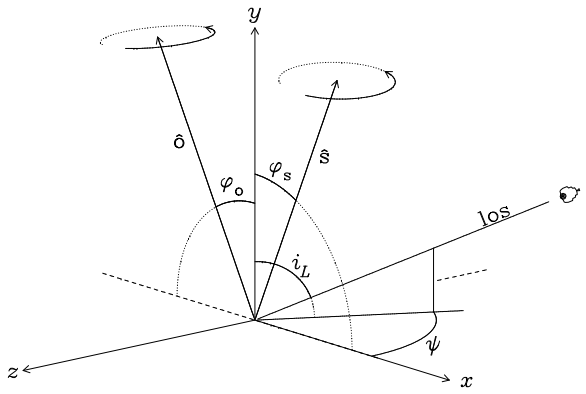

Figure 1. Spin-orbit geometry; the y axis coincides with **L**, the sum of the orbital and stellar-rotation angular momenta (unit vectors $\hat{\mathbf{o}}$, $\hat{\mathbf{s}}$), which lie in the xy plane. The line of sight, 'los', is shown for precessional phase ψ; it is offset from the total angular-momentum vector **L** by the angle i_L. The observer's-frame inclination angles i_o (between the line of sight and $\hat{\mathbf{o}}$) and i_s (between the line of sight and $\hat{\mathbf{s}}$) are not shown explicitly.

Orbital motion is retrograde with respect to the stellar rotation for $\varphi_s + \varphi_o > \pi/2$, prograde otherwise (where the φ angles are defined in Fig. 1).

Simple precession amounts to a rotation of **o** and **s** about **L**; observationally, this is equivalent to counter-rotation of the line of sight. Rather than impose a physical model of precession (which requires assumptions about quantities such as the stellar moment of inertia), in the present work the precessional angle ψ is left as a free parameter for each epoch of observation.

2.2.2 Stellar properties

Barnes et al. (2013) approximated the geometry of the rotationally distorted star by an oblate spheroid; here, the stellar surface is computed as a time-independent Roche equipotential (cf., e.g., Howarth & Smith 2001), neglecting any gravitational effects of the companion. The global effective temperature is defined by

$$T_{\rm eff}^4 = \int T_{{\rm eff}(\ell)}^4 \, {\rm d}A \Big/ \int {\rm d}A$$

where the integrations are over the distorted surface area, taking into account gravity darkening. For very rapid rotators this may not correspond to any particular 'observed' temperature (since the integrated line and continuum spectra will not precisely match any single-star standards), but it is at least a well-defined quantity.

Values of $T_{\rm eff} = 3470$ K and polar gravity $\log(g) = 4.0$ (cgs) are adopted here, following Briceño et al. (2005) and Barnes et al. (2013). These values enter the analysis *only* through the calculation of the surface intensities, discussed below; otherwise, no assumptions are made, or are required, in respect of specific values of the mass or polar radius, and other reasonable choices for $\log(g)$ would have no important effect on the results.

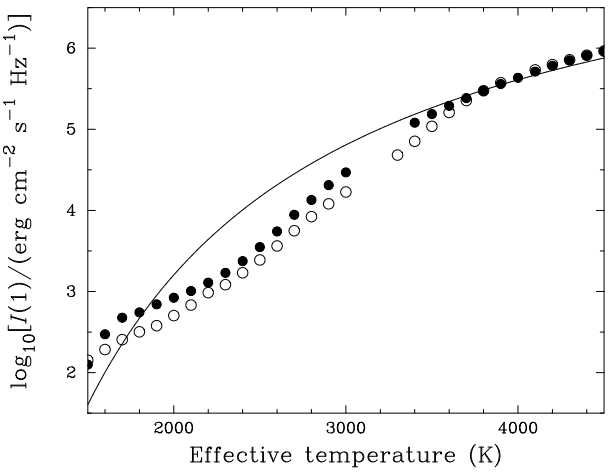

Figure 2. The R-band surface-normal intensity as a function of effective temperature. Filled and open circles are solar-abundance model-atmosphere results for $\log(g) = 4.5$ and 2.5 dex cm s^{-2}, respectively; the continuous curve is the (monochromatic) black-body result. Note that the y scale is logarithmic; the model-atmosphere intensities can show large departures from black-body behaviour.

2.2.3 Intensities

Since the temperature and surface gravity must vary significantly over the stellar surface (in order to generate the observed transit-curve asymmetries), the dependence of the emergent intensity on these quantities is of interest. In this work, R-band surface intensities were evaluated as $I(\mu, T_{\rm eff(\ell)}, g)$ by interpolation in the 'quasi-spherical' limb-darkening coefficients (LDCs) published by Claret, Hauschildt & Witte (2012), supplemented by surface-normal intensities kindly provided by Antonio Claret. His 4-coefficient LDC parametrization (Claret 2000), which reproduces the actual $I(\mu)$ distributions extremely well, was used.

The intensities derive from solar-abundance, line-blanketed, non-LTE PHOENIX model atmospheres (cf. Claret et al. 2012). Fig. 2 shows that the model-atmosphere emissivities can depart substantially from black-body results, by up to a factor ∼10 at 2.5 kK. Thus although the principal intention of the present analysis is to consider the consequences of an appropriate treatment of gravity darkening, the use of model-atmosphere intensities also represents a noteworthy if minor technical improvement over previous work, which adopted black-body fluxes coupled to a single, global, two-parameter limb-darkening law.

For the Barnes et al. (2013) best-fit models, the implied equator–pole temperature range is ∼3650–3350 K (for $T_{\rm eff}$ = 3470 K); over this temperature range, the model-atmosphere R-band surface-normal intensity ratio is ∼0.47, while the black-body ratio is ∼0.57. Relaxing the assumption of black-body emission is therefore liable to counteract the drive to larger values of $\omega/\omega_{\rm c}$ required by adopting a smaller value for the β exponent.

Table 1. Summary of Markov-chain Monte-Carlo results, for gravity darkening fixed at $\beta = 0.08$.

Parameter	Distribution		[Best]
$R_{\rm s}/a$	0.518	$^{+0.023}/_{-0.031}$	0.515
$R_{\rm p}/a$	0.1050	$^{+0.0087}/_{-0.0094}$	0.1045
$\omega/\omega_{\rm c}$	0.954	$^{+0.012}/_{-0.015}$	0.953
$i_L(^\circ)$	111.9	$^{+3.6}/_{-4.8}$	111.6
$\varphi_{\rm o}(^\circ)$	0.8	$^{+2.0}/_{-0.7}$	0.2
$\varphi_{\rm s}(^\circ)$	108.2	$^{+7.7}/_{-4.9}$	110.2
$\psi(^\circ, 2009)$	272.1	$^{+2.7}/_{-2.4}$	272.1
$\psi(^\circ, 2010)$	298.1	$^{+5.1}/_{-4.3}$	298.8
$\varphi_{\rm o} + \varphi_{\rm s}(^\circ)$	109.1	$^{+7.6}/_{-4.5}$	110.4
$i_{\rm s}(^\circ, 2009)$	81.4	$^{+2.8}/_{-3.2}$	80.8
$i_{\rm s}(^\circ, 2010)$	57.9	$^{+4.4}/_{-4.9}$	56.8
$i_{\rm o}(^\circ, 2009)$	111.9	$^{+3.6}/_{-4.8}$	111.6
$i_{\rm o}(^\circ, 2010)$	112.3	$^{+3.8}/_{-4.8}$	111.7

'Distribution' results are the median and 95% confidence intervals (from 10^6 MCMC replications), while the final column lists values for the individual trial model yielding the smallest rms residuals. $R_{\rm s}/a$ and $R_{\rm p}/a$ are the stellar polar radius and the planetary radius in units of the orbital semi-major axis; $\omega/\omega_{\rm c}$ is the ratio of stellar angular rotation to the critical value. Angles are defined in Fig. 1; the sum $\varphi_{\rm o} + \varphi_{\rm s}$, and the stellar-rotation & orbital inclinations, $i_{\rm s}$ & $i_{\rm o}$, are derived quantities, not free parameters in the model.

3 ANALYSIS

3.1 Observations

van Eyken et al. (2012) reported R-band observations of 11 separate transits in the 2009/10 observing season, and a further six in December 2010. Barnes et al. (2013) detrended and averaged these results to produce mean '2009' and '2010' light-curves. In order to approach as close as reasonably possible a like-for-like comparison with their results, the Barnes et al. composite light-curves were digitized and form the basis of the present analysis; the Barnes et al. ephemeris is consequently also adopted, as a fixed quantity. Because the dispersion in the data appears not to be purely stochastic, all points were equally weighted.

3.2 Methodology

In the model, the stellar geometry is determined by $\omega/\omega_{\rm c}$ and by $R_{\rm s}/a$, the polar radius expressed in units of the orbital semi-major axis; the exoplanet is characterized by its normalized radius, $R_{\rm p}/a$. Orbital/viewing geometry is defined by the angles $\varphi_{\rm o}$, $\varphi_{\rm s}$, i_L, and ψ (Fig. 1). The analysis requires all free parameters to be the same at both epochs of observation, excepting the viewing angles ψ.

Preliminary comparisons between the model and observations were carried out by using a simple grid search, guided by the Barnes et al. (2013) results. This pilot survey of parameter space was followed by a Markov-chain Monte-Carlo (MCMC) analysis using a standard Metropolis-Hastings algorithm (defaulting to 10^6 replications and uniform priors).

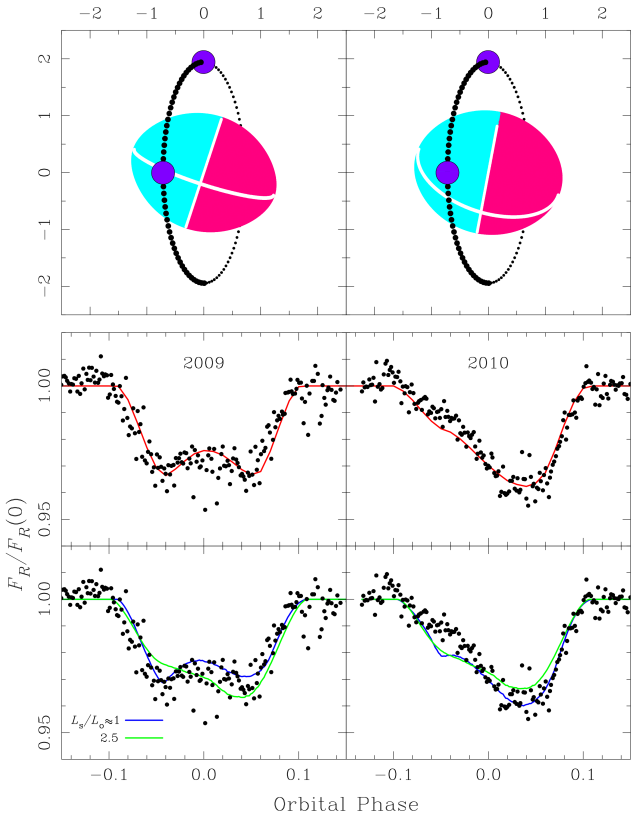

Figure 3. *Upper panels:* system geometry at the two epochs, for the 'best' solution summarized Table 1; the unit of length is the polar radius. The colour coding of blue- and red-shifted stellar hemispheres corresponds to prograde rotation; retrograde rotation would give rise to identical light-curves, as would mirror images of these panels. The locations of the transiting body at orbital phases 0.0 and 0.25 are shown, to indicate the direction of orbital motion. The projection of the total angular-momentum vector onto the plane of the sky is aligned with the $-x$ axis in each panel (and almost coincides with the orbital angular-momentum vector).
Centre panels: corresponding normalized model R-band light-curves and observations.
Bottom panels: the poorer 'best-fit' models obtained with angular-momentum ratios L_s/L_o constrained to values of 1 and 2.5 (q.v. §4.2).

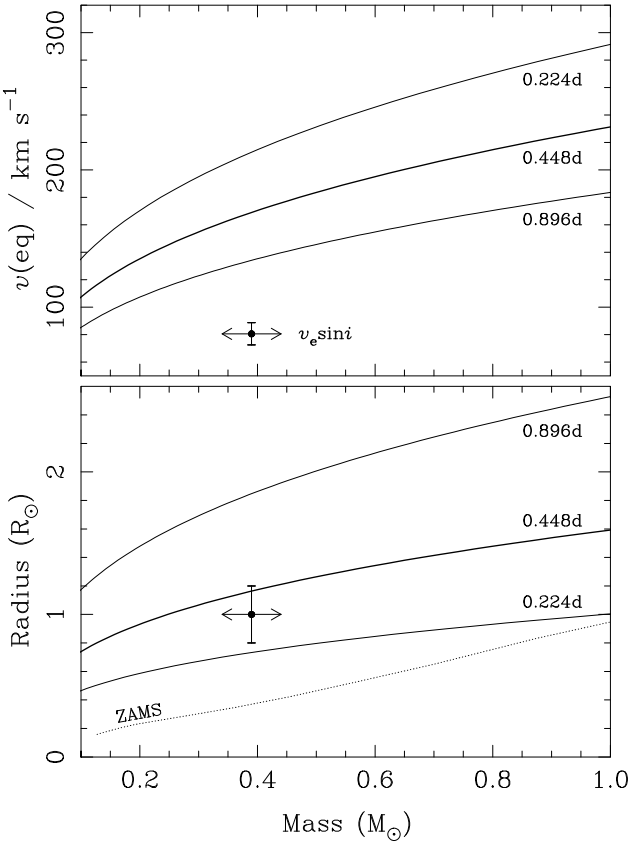

Figure 4. *Upper panel:* Equatorial rotation velocity as a function of mass, for $\omega/\omega_c = 0.954$ and three possible rotation periods. The $v_e \sin i_s$ measurement reported by van Eyken et al. (2012) is shown (with its 1-σ error) at the mass range adopted by Barnes et al. (2013).
Lower panel: corresponding polar radii, together with the ZAMS mass–radius relationship (following Eker et al. 2015; Bertelli et al. 2008). The photometric polar radius of $\sim 1.0 \pm 0.2$ R$_\odot$ is indicated (§4).

3.3 Results

A test run with $\beta = 0.25$ initially recovered essentially the same geometry as found by Barnes et al. (2013), although after $\sim 3 \times 10^5$ MCMC replications the fit migrated to an unphysical (though statistically marginally better) solution, involving a grazing transit of a planet $\sim 5\times$ larger than its parent star.

The $\beta = 0.08$ run did not suffer this problem, returning the parameter set summarized in Table 1. Fig. 3 illustrates the implied geometry, and confronts the predicted light-curve with the data. Disappointingly, the technical improvements to the basic Barnes et al. (2013) model implemented here lead to a somewhat poorer overall match than they achieved. In part, this is a consequence of requiring a consistent parameter set at both epochs (the two datasets can be matched extremely well if modelled separately, as one might expect, given the number of free parameters), but it is also suggestive of possible limitations of the model.

4 DISCUSSION

Phenomenologically, the solution obtained here provides a reasonably satisfactory match between observed and predicted normalized light-curves; however, it has *physical* implications which cast doubt on the completeness, or correctness, of the underpinning model.

4.1 Angular-momentum expectations

The magnitude of the stellar-rotation angular momentum for a star of mass M_s and polar radius R_s is

$$L_s = I\omega \simeq \beta_g^2 M_s R_s^2 \omega$$

where I is the moment of inertia, ω is the rotational frequency, and β_g is the fractional radius of gyration. A non-rotating 0.4M$_\odot$ star approaching the zero-age main sequence

has $\beta_g^2 \simeq 0.19$ (Claret 2012), giving

$$\frac{L_s}{\mathrm{kg\ m^2\ s^{-1}}} = 1.58 \times 10^{43} \left[\frac{M_s}{0.4\mathrm{M}_\odot}\right]^{3/2} \left[\frac{R_s}{\mathrm{R}_\odot}\right]^{1/2} \left[\frac{\omega}{\omega_c}\right] \left[\frac{\beta_g^2}{0.19}\right]$$

where each bracketed term is intended to be of order unity (using values for mass and radius based on discussions in van Eyken et al. 2012 and Barnes et al. 2013).

The magnitude of the planetary-orbit angular momentum for a planet of mass M_p with semi-major axis a and orbital frequency $\omega_{orb}(= 2\pi/P_{orb})$ is

$$L_o = M_p a^2 \omega_{orb},$$

$$\simeq M_p M_s^{2/3} P_{orb}^{1/3} \left[\frac{G}{\sqrt{2\pi}}\right]^{2/3} \quad (\text{for } M_p \ll M_s);$$

numerically, for $P_{orb} = 0.4484$d (van Eyken et al. 2012),

$$\frac{L_p}{\mathrm{kg\ m^2\ s^{-1}}} = 1.47 \times 10^{42} \left[\frac{M_p}{3\mathrm{M}_\downarrow}\right] \left[\frac{M_s}{0.4\mathrm{M}_\odot}\right]^{2/3}$$

whence the rotational:orbital angular-momentum ratio is

$$\frac{L_s}{L_o} \simeq 10.7 \left[\frac{\beta_g^2}{0.19}\right] \left[\frac{\omega}{\omega_c}\right] \left[\frac{M_s}{0.4\mathrm{M}_\odot}\right]^{5/6} \left[\frac{R_s}{\mathrm{R}_\odot}\right]^{1/2} \left[\frac{3\mathrm{M}_\downarrow}{M_p}\right].$$

The major source of uncertainty in this ratio is the planetary mass, which is constrained only by the van Eyken et al. upper limit ($M_p \leq [5.5 \pm 1.4]\mathrm{M}_\downarrow$), but the bracketed terms are, cumulatively, unlikely to differ from unity by more than perhaps a factor ∼3 or so.[4]

4.2 Angular-momentum results

The empirical results summarized in Table 1, obtained in the absence of any constraint on the angular-momentum ratio, yield

$$\frac{L_s}{L_o}\left[\equiv \frac{\sin(\varphi_p)}{\sin(\varphi_s)}\right] = 0.014^{+0.036}_{-0.013}$$

(median, 95% confidence intervals). This is discrepant, by almost three orders of magnitude, with the prediction of §4.1; furthermore, the negligible orbital precession implied by the small value of φ_o is inconsistent with the absence of transits at some epochs (e.g., Kamiaka et al. 2015).

Reasonably extensive sampling of parameter space, including several tens of millions of MCMC replications starting from multiple initial parameter sets, encourages the view that the solution summarized in Table 1 locates the global minimum in χ^2 hyperspace. However (and particularly given that the model is constrained by observations only two epochs), the question arises as to whether a physically better model may exist with lower, but still acceptable, statistical probability – that is, does a preferable solution occur at a local χ^2 minimum?

To investigate this issue, further solutions were sought, again through the MCMC process but imposing a variety of constraints on the L_s/L_o ratio. In all these experiments, the angular-momentum ratio was found always to drive towards the smallest allowed values. Figure 3 illustrates the outcomes of two such experiments, one in which L_s/L_o was fixed at the Barnes et al. value of 2.5, and one in which it was required to be ≥1 (with the outcome that the chain settled on a value very close to 1). Neither of these models, nor any others examined, can be considered as giving satisfactory fits.

4.3 Consequences of stellar precession

In the basic Barnes et al. (2013) model explored here, a large part of the light-curve variability between epochs arises through precessional 'nodding' of the star (almost independently of the orbital angular-momentum issue discussed above). This nodding gives rise to two potentially observable diagnostics. First, because of changes in $\sin i_s$, variability is expected in the projected equatorial rotation velocity, $v_e \sin i_s$ (by a factor ∼ 1.2 between the 2009 and 2010 epochs). This may be easier to study spectroscopically than the Rossiter–McLaughlin effect, because the variability timescale is very much longer (allowing acquisition of better data).

Secondly, because the hotter polar regions of the star are presented towards the observer in 2010, the system is predicted to be brighter, by as much as $\Delta R = 0\overset{m}{.}30$ for the 'best' solution of Table 1. The PTFO photometry is in clear contradiction with this prediction. Although there is significant non-orbital variability, the observations shown by van Eyken et al. (2012) fall in the range $R \simeq 15.20 \pm 0.05$ at both 2009 and 2010 epochs (their Figs. 2 and 3; the *extreme* peak-to-peak range is only $0\overset{m}{.}17$). This is a strong argument against the basic foundation of the Barnes et al. model: any significant changes in the transit morphology resulting from precession of a gravity-darkened star are necessarily accompanied by changes in the overall brightness[5] – which is not observed.

4.4 Stellar rotation

As anticipated, the solution with $\beta = 0.08$ requires a large (and reasonably well-defined) value for ω/ω_c. The associated values of stellar mass, radius, and equatorial rotation are not independent, but it is straightforward to compute consistent sets of values for given ω/ω_c and rotation period P_{rot}. van Eyken et al. (2012) found a signal with $P = 0.448$ d in out-of-transit photometry, suggesting the possibility of approximate rotational/orbital synchronization; Fig. 4 illustrates the stellar equatorial rotation velocity and polar radius as functions of mass for this P_{rot}, and for values that are a factor two different in each direction.

For $V_0 \simeq 16.1$, $T_{eff} \simeq 3.5$ kK, and $d \simeq 330$ pc (Briceño et al. 2005), the effective stellar radius must be $\sim 1.1 \pm 0.2$ $\mathrm{R}_\odot$ (polar radius $\sim 1.0 \pm 0.2$ $\mathrm{R}_\odot$), as judged from MARCS and ATLAS model-atmosphere fluxes (Gustafsson et al. 2008; Howarth 2011; see also Barnes et al. 2013). Supposing the stellar mass to be $\sim 0.4 \pm 0.05$ $\mathrm{M}_\odot$ (Briceño et al. 2005; Barnes et al. 2013), rotation must indeed be close to, or somewhat faster than, synchronous to match this radius (Fig. 4), which in turn implies an equatorial rotation velocity $v_e \gtrsim 160$ km s^{-1}.

[4] The Barnes et al. (2013) 'joint solution' (their Table 3) has $L_s/L_o \simeq 2.5$, consistent with their adoption of the Solar value for squared normalised radius of gyration (the 'moment of inertial coefficient' in their terminology), $\beta_g^2 = 0.059$.

[5] The Barnes et al. $\beta = 0.25$ solution implies $\Delta R \simeq 0\overset{m}{.}2$.

van Eyken et al. (2012) report $v_{\rm e} \sin i_{\rm s} = 80.6 \pm 8.1$ km s^{-1} from observations obtained in 2011 February. If we suppose the inclination at that epoch to be close to the 2010 December value, then $v_{\rm e} \simeq 95$ km s^{-1}. Rapid rotation may lead to underestimation of $v_{\rm e} \sin i_{\rm s}$ (because a consequence of gravity darkening is relatively low visibility of equatorial regions; cf., e.g., Townsend, Owocki & Howarth 2004), but the discrepancy between observed and expected equatorial velocities is too large to be explained by this effect. Though less secure than the photometric constraint, this is therefore a further source of conflict between the model and observations.

5 CONCLUSION

The ingenious 'precession + gravity darkening' model proposed by Barnes et al. (2013) to interpret transit photometry of PTFO 8-8695 has been tested using a more appropriate characterization of gravity darkening, along with with more sophisticated treatments of surface intensities and stellar geometry.

Although the normalized transit light-curves can still be adequately reproduced by the model, the solution offered here has an implausibly small ratio of rotational to orbital angular momenta. While other, physically more acceptable solutions are not completely ruled out, reasonably extensive exploration of parameter space has failed to locate any such solution.

Independently of this issue, the adoption of a smaller gravity-darkening exponent than previously assumed leads inexorably to the requirement of near-critical stellar rotation. Such rapid rotation raises two further, and more general, difficulties for the model. First, given the 'known' radius, the projected rotational velocity is predicted to be approaching a factor two greater than observed. Secondly, a substantially gravity-darkened star must exhibit significant photometric variability associated with precession of the rotation axis; no such variability is observed.

Collectively, these results suggest that either the basic model omits important physics, or that a conventional transiting exoplanet is not the correct explanation for the fading events in the PTFO 8-8695 system.

ACKNOWLEDGMENTS

I thank Antonio Claret for kindly providing absolute intensities to supplement his published limb-darkening coefficients; Ingo Waldmann & Michel Rieutord for enlightening discussions; and Jason Barnes & Julian van Eyken for helpful exchanges (the former both as pre-submission correspondent and constructive referee).

REFERENCES

Barnes J. W., van Eyken J. C., Jackson B. K., Ciardi D. R., Fortney J. J., 2013, ApJ, 774, 53
Bertelli G., Girardi L., Marigo P., Nasi E., 2008, A&A, 484, 815
Briceño C., Calvet N., Hernández J., Vivas A. K., Hartmann L., Downes J. J., Berlind P., 2005, AJ, 129, 907
Ciardi D. R., et al., 2015, ApJ, 809, 42
Claret A., 2000, A&A, 363, 1081
Claret A., 2012, A&A, 541, A113
Claret A., Hauschildt P. H., Witte S., 2012, A&A, 546, A14
Djurašević G., Rovithis-Livaniou H., Rovithis P., Georgiades N., Erkapić S., Pavlović R., 2003, A&A, 402, 667
Djurašević G., Rovithis-Livaniou H., Rovithis P., Georgiades N., Erkapić S., Pavlović R., 2006, A&A, 445, 291
Eker Z., et al., 2015, AJ, 149, 131
Espinosa Lara F., Rieutord M., 2011, A&A, 533, A43
Gustafsson B., Edvardsson B., Eriksson K., Jørgensen U. G., Nordlund Å., Plez B., 2008, A&A, 486, 951
Howarth I. D., 2011, MNRAS, 413, 1515
Howarth I. D., Smith K. C., 2001, MNRAS, 327, 353
Kamiaka S., et al., 2015, PASJ, 67, 94
Lucy L. B., 1967, Z. Astrophys., 65, 89
Pantazis G., Niarchos P. G., 1998, A&A, 335, 199
Rafert J. B., Twigg L. W., 1980, MNRAS, 193, 79
Rieutord M., 2015, preprint, (arXiv:1505.03997)
Townsend R. H. D., Owocki S. P., Howarth I. D., 2004, MNRAS, 350, 189
Yu L., et al., 2015, ApJ, 812, 48
van Eyken J. C., et al., 2011, AJ, 142, 60
van Eyken J. C., et al., 2012, ApJ, 755, 42
von Zeipel H., 1924, MNRAS, 84, 665